two types of such module sequences: [1,0] or [1,0] and [1,1], respectively, may be considered as homogeneous arising from module-by-module crystal growth, whereas the HS defects proceed by some violation of the growth conditions.

Some general diffraction features of oxyborate structures

Common lattice features in direct space are accordingly represented in reciprocal space and, hence, in diffraction patterns. Most distinctly, such features are displayed in selected-area electron diffraction (SAED) patterns of single crystals. The set of coordinate axes in the reciprocal space is defined by the relationship between linear transformations of axes in both spaces as $\mathbf{a}^* = \mathbf{a}_o^* - (m/5n)\mathbf{c}_o^*$, $\mathbf{b}^* = \mathbf{b}_o^*$, $\mathbf{c}^* = \mathbf{c}_o^*/n$. According to these equations, any electron-diffraction patterns obtained from a single crystal in orientation with the b axis parallel to the incident beam images the reciprocal lattice plane $\mathbf{a}^*\mathbf{c}^*$. This pattern contains $h0l$ reflections distributed along rows having constant h and variable l indices. The separations between the rows are proportional to $1/a_o$, and the intervals between the reflections of the row are proportional to $1/(nc_o)$. The consecutive reflections $h00$ are displaced along their rows by $-mc^*/5 = -m/(5nc_o)$, in accordance with the relationship $a^*\cos\beta^* = -m/5$. At the choice of other axes a' giving β'-angles closer to 90°, the c'^* axis unites reflections of different rows. In the particular case of $m = -1$, $n = 1$, $\mathbf{a}'^* = \mathbf{a}^*$, $\mathbf{c}'^* = -\mathbf{a}^* + \mathbf{c}^*$ (Fig. 4). The transformation of indices being covariant with the transformation of axes in the direct space is accordingly $h' = h + 1$, $k' = k$, $l' = l$.

Concluding remarks

The application of the modular approach has provided a clear and simple understanding of the variations in oxyborate structures. At the same time, it has displayed almost all the general features of the modular approach: choice of modules; formulation of the stacking rules; use of symbolic notations as a simple means for operation with structures; derivation of homogeneous structures and presentation of inhomogeneous structures as combinations of the homogeneous ones; treatment of all individual structures as members of a united system considered relative to common coordinate axes in the direct and reciprocal spaces and in diffraction patterns. In the view of the modular approach, the concepts of 'slip' and 'twinning' seem redundant for explaining the oxyborate structural variations.

This work has been supported by the Russian Foundation of Fundamental Studies (RFS Project 93-05-14248). The authors are also grateful to J.-O. Bovin and to the unidentified referees whose remarks and recommendations served for essential refinement of this text.

References

ALFREDSSON, V., BOVIN, J.-O., NORRESTAM, R. & TERASAKI, O. (1991). *Acta Chem. Scand.* **45**, 797–804.
BOVIN, J.-O., O'KEEFE, M. & O'KEEFE, M. A. (1981). *Acta Cryst.* A**37**, 28–35.
DORNBERGER-SCHIFF, K. (1964). *Grundzüge einer Theorie der OD-Strukturen aus Schichten*. Berlin: Abh. Deutsch. Akad. Wiss.
DORNBERGER-SCHIFF, K. (1982). *Acta Cryst.* A**38**, 483–491.
DORNBERGER-SCHIFF, K. & GRELL, H. (1982). *Acta Cryst.* A**38**, 491–498.
DUROVIC, S. (1992). *International Tables for Crystallography*, Vol. C, pp. 667–680. Dordrecht: Kluwer Academic Publishers.
RAADE, G., MLADECK, M. H., DIN, V. K., GRIDDLE, A. J. & STANLEY, C. J. (1988). *Neues Jahrb. Mineral. Monatsh.* **3**, 121–136.
TAKEUCHI, Y., HAGA, N., KATO, T. & MIARA, Y. (1978). *Can. Mineral.* **16**, 475–485.
ZHDANOV, G. S. (1945). *Dokl. Akad. Nauk SSSR*, **48**, 40–43.
ZVYAGIN, B. B. (1988). *Comput. Math. Appl.* **16**, 569–591.
ZVYAGIN, B. B. (1993). *Crystallogr. Rep.* **38**, 54–60.
ZVYAGIN, B. B. & BELOKONEVA, E. L. (1984). *Sov. Phys. Crystallogr.* **29**, 173–176.
ZVYAGIN, B. B. & ROMANOFF, E. G. (1991). *Sov. Phys. Crystallogr.* **36**, 75–80.

Acta Cryst. (1995). **B51**, 11–18

The Structures of α- and β-$Bi_2Ti_4O_{11}$

BY V. KAHLENBERG AND H. BÖHM

Institut für Geowissenschaften (Mineralogie), Johannes Gutenberg Universität, 55099 Mainz, Germany

(*Received* 12 *March* 1994; *accepted* 22 *April* 1994)

Abstract

The phase transition and the crystal structures of $Bi_2Ti_4O_{11}$ have been investigated by X-ray diffraction. The compounds possess the following parameters: α-$Bi_2Ti_4O_{11}$: monoclinic, space group $C2/c$, $a = 14.5999(6)$, $b = 3.8063(2)$, $c = 14.9418(8)$ Å, $\beta = 93.129(4)°$, $V = 829.1(1)$ Å^3, $Z = 4$,

D_x = 6.29 g cm^{-3}, Mo $K\alpha$, μ = 44.31 mm^{-1}, wR = 0.029 for 2361 reflections; β-$Bi_2Ti_4O_{11}$: monoclinic, space group $C2/m$, a' = 14.6412 (12), b' = 3.8032 (3), c' = 10.7824 (6) Å, β = 136.135 (5)°, V = 416.06 (10) Å^3, T = 573 K, Z = 2, wR = 0.043 for 1204 reflections. The transformation at 506 K leads from a paraelectric high-temperature modification (β-$Bi_2Ti_4O_{11}$), with the space group $C2/m$, to a $C2/c$ antiferroelectric low-temperature phase (α-$Bi_2Ti_4O_{11}$) and is induced by a displacement of the Bi atoms at *ca* 0.29 Å along [010] in the channels of the Ti—O network. For the description of the transition, it is convenient to transform the unit cell of α-$Bi_2Ti_4O_{11}$ according to $\mathbf{a}'' = \mathbf{a}, \mathbf{b}'' = \mathbf{b}, \mathbf{c}'' = -\mathbf{a} + \mathbf{c}$. In this new setting, the position of superlattice reflections results in a cell doubling parallel [001], indicating a phonon condensation at the A-point $[00\frac{1}{2}]$ on the boundary of the Brillouin zone of $C2/m$. A symmetry analysis has been performed based on the Landau formalism and projection operator methods. The displacements parallel and antiparallel to **b** were taken as the primary-order parameter, which transforms according to the irreducible representation A_2^+ .

Introduction

The existence and some physical properties of bismuth tetratitanate, $Bi_2Ti_4O_{11}$, were first reported by Subbarao (1962). The temperature dependence of the thermal expansion and the dielectric data measured on ceramic discs indicated a phase transition at *ca* 523 K. The transition is not ferroelectric since the dielectric hysterisis and the piezoelectric response have not been observed. Hisano & Toda (1977) investigated the temperature dependence of the Raman active modes in $Bi_2Ti_4O_{11}$ and found that the lowest frequency mode near 38 cm^{-1} underwent a considerable softening on approaching 495 K from below their determined transition temperature of 511 K. The powder X-ray diffraction diagram of the high-temperature modification was reported by Mitrovich & Blinov (1982). Single crystals of $Bi_2Ti_4O_{11}$ have been grown by hydrothermal crystallization and from oxide melts (Barsukova, Kuznetsov, Lobachev & Tanakina, 1973; Shimada, Kodaira & Matsushita, 1977). The crystal structure of $Bi_2Ti_4O_{11}$ at room temperature has been reported as monoclinic with the space group $B2/b$ and lattice constants a = 14.604, b = 14.943, c = 3.8049 Å, and γ = 92.10° by Petushkova, Dmitrieva, Pobedimskaya & Belov (1974). The refinement led to an unsatisfactory result with negative isotropic temperature factors for the Ti atoms and some O atoms. The model of α-$Bi_2Ti_4O_{11}$ indicates a pseudo-symmetry. We decided to re-examine this bismuth titanate compound because little is known about the structures and the mechanism of the phase transition.

Experimental

The powder samples of $Bi_2Ti_4O_{11}$ ($Bi_2O_3.4TiO_2$) have been synthesized from Bi_2O_3 (99.9%) and TiO_2 (99.8%, anatase). The reagents were carefully mixed in an agate mortar and pressed into discs (10 mm diameter × 1.0 mm thickness) under a pressure of 8.13 × 10^3 kg cm^{-2}. The mixtures confined in covered platinum crucibles were heated in air at several temperatures (1223–1473 K) for various periods of time up to 13 h, and cooled rapidly in air. Because of the considerable weight loss (>1 wt %) due to volatilization of the Bi_2O_3 component for reaction temperatures above 1373 K, the sample material for the X-ray powder diffraction investigations was taken from the 1223 K specimen.

The single crystals used in the present study were grown in platinum crucibles from a Bi_2O_3 flux. In order to reduce the corrosive properties of Bi_2O_3, which is known to attack platinum severely, V_2O_5 (99.5%) was added to guarantee oxidizing conditions (Pamplin, 1974). Powder mixtures of 5 g were placed in covered 50 ml platinum crucibles. The starting material was heated in air from 373 K in 8 h to 1473 K, held at this temperature for 24 h to homogenize the melt and cooled down to 1148 K at a rate of 5 K h^{-1}. After cooling, the melt was immediately quenched. The grown needle-shaped crystals could be mechanically separated from the remaining flux. The best results with respect to the dimensions of the crystals were obtained for a nutrient:flux weight ratio of 1:3.57 and a flux composition $V_2O_5.3Bi_2O_3$. The composition of the crystals was determined with an electron beam microprobe from Cameca; it did not vary from the ideal stoichiometry.

The thermoanalytical measurements were made on a Perkin–Elmer DSC-7 calorimeter. High-temperature powder diffraction experiments were carried out on a Huber 632 Guinier powder camera using Cu $K\alpha$ radiation from a curved germanium monochromator. The employed asymmetric transmission geometry allowed the recording of reflections up to a diffraction angle θ of 60°. In consequence of the high absorption coefficient for the materials, the $Bi_2Ti_4O_{11}$ powder was diluted with silica gel. For temperature calibration, the phase transitions and the melting point of KNO_3 were used.

For the single-crystal investigations, a crystal of good optical quality was selected and ground to a sphere with 0.2 mm diameter. The study of the phase transition on a precession camera and a single crystal diffractometer, respectively, was performed by means of two different heating devices based on the principle of immersing the crystal in a hot gas stream, as described by Tuinstra & Storm (1978) and Kahlenberg & Böhm (1992). The crystal was mounted with a ceramic cement on the tip of a quartz glass capillary (0.2 mm diameter) held in a brass rod. The cement was preheated for 2 h at 393 K and then a second capillary of 0.5 mm diameter was slid over the first in order to eliminate vibrations of

the inner capillary due to the laminary nitrogen flow. The temperature was measured using a chromel–alumel thermocouple mounted on an *xy* stage.

The measurements of the single-crystal intensities were performed using an Enraf–Nonius CAD-4 four-circle diffractometer with graphite monochromated Mo $K\alpha$ radiation in the ω–2θ-step scan mode (see Table 1).* For the determination of the lattice parameters, 25 reflections with $20 \le \theta \le 35°$ were used. Intensity and orientation of three standard reflexions were regularly monitored. Psi-scans were performed to check absorption effects (nine reflections, 10° increment). Nearly constant transmission was observed, proving the good spherical shape of the crystal.

Lorentz–polarization and spherical absorption corrections ($\mu R = 4.43$) were applied using the program system *MolEN* (Enraf–Nonius, 1990). Other computer programs used in the course of this investigation were *SHELX*76 (Sheldrick, 1976) for structure solution and refinement, *SADIAN*91 (Baur, Wenninger, Roy & Kassner, 1986) for determination of interatomic distances and angles and *STRUPLO*90 (Fischer, LeLirzin, Kassner & Rüdinger, 1990) for drawing details. Atomic scattering factors and real and imaginary anomalous-dispersion coefficients were taken from *International Tables for X-ray Crystallography* (Ibers & Hamilton, 1974). The refinements were calculated by full-matrix least squares, minimizing the function $\Sigma w(|F_o| - |F_c|)^2$ $\{w = 1/[\sigma(F)^2]\}$. No extinction correction was applied.

Structural analysis of $Bi_2Ti_4O_{11}$

Precession and Laue photographs indicated the monoclinic Laue symmetry 2/*m*. The systematic absences (*hkl*), $h + k = 2n + 1$ and (*h*0*l*), $l = 2n + 1$ resulted in the two possible space groups *Cc* or *C*2/*c*. A three-dimensional sharpened Patterson synthesis revealed the coordinates of the Bi ions. The concentration of interatomic vectors in the Harker section (*x*0*z*), in combination with the negative outcome of a test for piezoelectricity, led to the choice of the centrosymmetric space group for α-$Bi_2Ti_4O_{11}$. The positions of the crystallographically different titanium ions Ti(1), Ti(2) and the six oxygen anions O(1)–O(6) were located by a series of subsequent Fourier calculations. Apart from O(3), occupying the special Wyckoff position 4(*e*), all other atoms were distributed over the general positions 8(*f*) of *C*2/*c*. A refinement starting from these atom coordinates converged to a final weighted residual of $wR = 0.029$ for all reflections with $I \ge 2\sigma_I$ and 78 variable parameters. The refined atomic coordinates, anisotropic displacement parameters, interatomic distances up to a maximal value of 3.4 Å and selected angles are given in Tables 2–5. In the structure of the α-phase, the titanium cations are coordinated by six nearest oxygen neighbours; the octahedra exhibit considerable distortion, especially that around Ti(1). The individual Ti—O distances vary between 1.797 and 2.200 Å for Ti(1) and between 1.879 and 2.007 Å for Ti(2), with mean Ti—O distances of 1.970 and 1.952 Å, respectively. The angles between the central atom and the corners of the octahedra show a pronounced deviation from the ideal values 180 and 90°.

According to investigations made by Tillmanns, Hofmeister & Baur (1985), large variation in the individual Ti—O distances for octahedral coordination is a widely known phenomenon and largely due to the differences in bond strengths of the O atoms. In comparison with the lower and upper limits of 1.723 and 2.456 Å, determined by Tillmanns, Hofmeister & Baur (1985), the present case shows no unusual scattering of the individual Ti—O distances.

The Bi atoms are surrounded by 11 O atoms with distances of up to 3.362 Å. The coordination number 12 given by Petushkova, Dmitrieva, Pobedimskaya & Belov (1974) is not confirmed by the present studies. Obviously, Bi—Ti distances which are shorter than the distance to the twelfth O atom were neglected by these authors. A more adequate description of the Bi coordination can be achieved by comparing our data with the results of Wells (1984), who noted that in many Bi^{3+} oxy-compounds the cation has an inner coordination sphere with five or six neighbours at distances of *ca* 2.1–2.7 Å (mean close to 2.4 Å) and an outer sphere with a number of additional neighbours. The present structure also belongs to this group, as can be seen in Table 4. The

Table 1. *Parameters for the X-ray data collection*

	α-$Bi_2Ti_4O_{11}$	β-$Bi_2Ti_4O_{11}$
Temperature (K)	296	573
a (Å)	14.5999 (6)	14.6412 (12)
b (Å)	3.8063 (2)	3.8032 (3)
c (Å)	14.9418 (8)	10.7824 (6)
β (°)	93.129 (4)	136.135 (5)
V (Å^3)	829.11 (7)	416.06 (10)
Range of *h*	$-26 \rightarrow 26$	$-26 \rightarrow 0$
k	$0 \rightarrow 6$	$-6 \rightarrow 0$
l	$0 \rightarrow 27$	$-19 \rightarrow 19$
$(\sin\theta/\lambda)_{max}$ (Å^{-1})	0.481	0.481
Measured reflections	2461	1314
Observed reflections	2361	1204
Observation criterion	$[I > 2\sigma(I)]$	$[I > 2\sigma(I)]$

Table 2. *Fractional atomic coordinates for* α-$Bi_2Ti_4O_{11}$

	x	*y*	*z*
Bi	0.3212 (1)	0.3251 (1)	0.1796 (1)
Ti(1)	0.0535 (1)	0.2499 (3)	0.1408 (1)
Ti(2)	0.1462 (1)	0.7410 (3)	0.0169 (1)
O(1)	0.0792 (3)	0.7479 (12)	0.1286 (3)
O(2)	0.1385 (3)	0.2461 (12)	0.0340 (3)
O(3)	0	0.2281 (23)	1/4
O(4)	0.2693 (3)	0.7366 (13)	0.0836 (3)
O(5)	0.4464 (3)	0.7470 (15)	0.0755 (3)
O(6)	0.1834 (3)	0.2564 (12)	0.2224 (3)

* A list of structure factors has been deposited with the IUCr (Reference: SE0149). Copies may be obtained through The Managing Editor, International Union of Crystallography, 5 Abbey Square, Chester CH1 2HU, England.

Table 3. *Anisotropic displacement parameters* ($Å^2$) *for* α-$Bi_2Ti_4O_{11}$

	U_{11}	U_{22}	U_{33}	U_{12}	U_{13}	U_{23}
Bi	0.0051 (1)	0.0069 (1)	0.0064 (1)	0.0001 (1)	0.0021 (1)	0.0008 (1)
Ti(1)	0.0034 (4)	0.0024 (4)	0.0038 (4)	−0.0001 (3)	0.0014 (3)	−0.0001 (3)
Ti(2)	0.0035 (3)	0.0029 (4)	0.0045 (4)	0.0000 (3)	0.0016 (3)	0.0000 (3)
O(1)	0.0067 (17)	0.0034 (17)	0.0064 (17)	0.0004 (14)	0.0044 (14)	−0.0004 (13)
O(2)	0.0080 (17)	0.0027 (17)	0.0075 (18)	0.0001 (14)	0.0039 (14)	−0.0008 (14)
O(3)	0.0092 (25)	0.0174 (36)	0.0057 (24)	0	0.0048 (20)	0
O(4)	0.0057 (16)	0.0090 (20)	0.0027 (15)	0.0031 (15)	0.0009 (13)	0.0001 (15)
O(5)	0.0052 (17)	0.0145 (23)	0.0091 (19)	0.0011 (17)	−0.0037 (15)	0.0006 (17)
O(6)	0.0038 (15)	0.0073 (19)	0.0048 (16)	0.0033 (14)	0.0013 (13)	0.0002 (13)

Table 4. *Interatomic distances up to a maximum of* 3.4 Å *for* α-$Bi_2Ti_4O_{11}$

Ti(1)–O(1)	1.943 (5)	Bi–O(1)	3.155 (5)
Ti(1)–O(5)	1.797 (5)	Bi–O(4)	2.229 (5)
Ti(1)–O(1)	1.958 (5)	Bi–O(6)	2.159 (4)
Ti(1)–O(6)	2.200 (4)	Bi–O(2)	3.289 (5)
Ti(1)–O(2)	2.075 (5)	Bi–O(4)	2.745 (5)
Ti(1)–O(3)	1.849 (1)	Bi–O(6)	2.202 (5)
Ti(2)–O(1)	1.980 (5)	Bi–O(2)	3.362 (5)
Ti(2)–O(4)	2.007 (4)	Bi–O(5)	2.941 (5)
Ti(2)–O(2)	1.905 (5)	Bi–O(6)	2.615 (5)
Ti(2)–O(5)	1.879 (5)	Bi–O(3)	3.158 (4)
Ti(2)–O(2)	1.943 (5)	Bi–O(5)	3.304 (5)
Ti(2)–O(4)	1.998 (4)		

Table 5. O—Ti—O *angles* (°) *for* α-$Bi_2Ti_4O_{11}$

O(1)—Ti(1)—O(1)	154.8 (2)	O(1)—Ti(2)—O(2)	80.9 (2)
O(1)—Ti(1)—O(3)	102.7 (3)	O(1)—Ti(2)—O(4)	170.8 (2)
O(1)—Ti(1)—O(5)	97.0 (2)	O(2)—Ti(2)—O(4)	89.0 (2)
O(2)—Ti(1)—O(3)	167.9 (1)	O(2)—Ti(2)—O(4)	100.7 (2)
O(3)—Ti(1)—O(5)	94.7 (2)	O(4)—Ti(2)—O(4)	78.5 (2)
O(1)—Ti(1)—O(2)	78.2 (2)	O(1)—Ti(2)—O(2)	82.3 (2)
O(1)—Ti(1)—O(3)	97.5 (3)	O(1)—Ti(2)—O(5)	104.5 (2)
O(1)—Ti(1)—O(6)	82.8 (2)	O(2)—Ti(2)—O(4)	90.0 (2)
O(2)—Ti(1)—O(6)	83.8 (2)	O(2)—Ti(2)—O(5)	91.6 (2)
O(3)—Ti(1)—O(6)	84.5 (1)	O(4)—Ti(2)—O(5)	84.0 (2)
O(1)—Ti(1)—O(2)	78.9 (2)	O(1)—Ti(2)—O(4)	93.0 (2)
O(1)—Ti(1)—O(5)	96.3 (2)	O(2)—Ti(2)—O(2)	163.0 (2)
O(1)—Ti(1)—O(6)	84.2 (2)	O(2)—Ti(2)—O(4)	95.7 (2)
O(2)—Ti(1)—O(5)	97.0 (2)	O(2)—Ti(2)—O(5)	94.5 (2)
O(5)—Ti(1)—O(6)	179.1 (2)	O(4)—Ti(2)—O(5)	162.4 (2)

inner coordination group of the five O atoms with Bi—O distances up to 2.745 Å form a square pyramidal group with a mean Bi—O bond length of 2.390 Å; the Bi^{3+} ion is located *ca* 0.20 Å in front of the pyramidal basis plane.

The octahedra build up a network with channels containing the Bi cations. For a description of the network it is convenient to choose double chains of Ti(1) and Ti(2) octahedra running in the [010] direction. The common edges are inclined with respect to the (010) plane. In a next step, a four-octahedra-wide ribbon can be constructed from two double chains sharing an edge which is almost parallel to the (010) plane. A slab parallel to the *ab* plane is the next largest building unit, which can be obtained from the connection of the ribbons *via* the O(5) atoms in the [100] direction (Fig. 1). The attachment of single slabs *via* common O(3) atoms completes the network. When looking 10° away from the direction of the short *b* axis, the network with the tunnels becomes clearly recognizable (Fig. 2).

The infinite octahedra chains parallel to [010] account for the needle-shaped crystal habit in this direction. The structure of α-$Bi_2Ti_4O_{11}$ is in some respects related to a series of alkali and barium titanates called Wadsley–Andersson phases (Andersson & Wadsley, 1962; Tillmanns, 1974). These compounds have a short cell constant of *ca* 4 Å and crystallize as needles. This value corresponds to the long diagonal of the TiO_6-octahedron. As in $Bi_2Ti_4O_{11}$, the structures contain infinite zigzag bands building channels which are occupied by the large Ba and alkali ions, but with a difference in the connection of the two- or three-octahedra-wide chains to bigger building units.

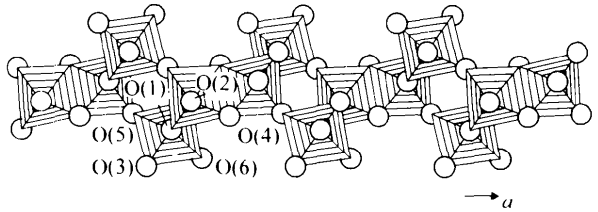

Fig. 1. Part of a single slab consisting of TiO_6-octahedra projected parallel to the [010] direction.

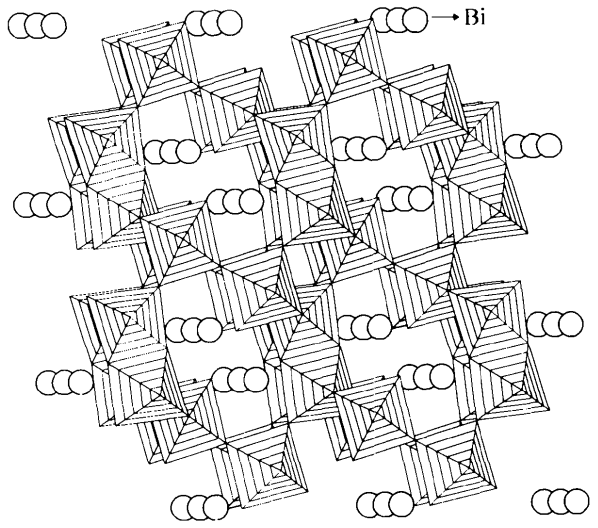

Fig. 2. Projection of α-$Bi_2Ti_4O_{11}$ deviating 10° from the [010] direction; the tunnels contain the Bi cations.

Table 6. *Relations between the shifted coordinates of* Ti(1) *in C2/c and F2/m*

x	*y*	*z*	*F2/m*-positions	
0.0533	¯0	−0.1092	(*x*0*z*)	+000
0.5533	¯1/2	−0.1092	(*x*0*z*)	$+\frac{1}{2}\frac{1}{2}0$
0.5533	¯0	0.3908	(*x*0*z*)	$+\frac{1}{2}0\frac{1}{2}$
0.0533	¯1/2	0.3908	(*x*0*z*)	$0\frac{1}{2}\frac{1}{2}$
0.9467	¯0	0.1092	(*x*̄0*z*̄)	+000
0.4467	¯1/2	0.1092	(*x*̄0*z*̄)	$+\frac{1}{2}\frac{1}{2}0$
0.4467	¯0	0.6092	(*x*̄0*z*̄)	$+\frac{1}{2}0\frac{1}{2}$
0.9467	¯1/2	0.6092	(*x*̄0*z*̄)	$+0\frac{1}{2}\frac{1}{2}$

Table 7. *Fractional atomic coordinates for* β-$Bi_2Ti_4O_{11}$

	x	*y*	*z*
Bi	0.2509 (1)	0	0.1421 (1)
Ti(1)	0.4449 (2	0	0.7828 (2)
Ti(2)	0.0871 (2)	0	0.4667 (2)
O(1)	0.4588 (9)	1\2	0.7582 (11)
O(2)	0.4255 (9)	0	0.5704 (12)
O(3)	1\2	0	0
O(4)	0.6036 (7)	1\2	0.6667 (10)
O(5)	0.2728 (8)	0	0.6503 (12)
O(6)	0.6558 (8)	0	0.9449 (10)

Pseudo-symmetry

An inspection of the *y*-coordinates in the network atoms Ti(1), Ti(2) and O(1)–O(6) reveals, interestingly, that they are concentrated near the planes $(x\frac{3}{4}z)$ and $(x\frac{1}{4}z)$. The largest deviation occurs at the position of the O(3) anion (y = 0.2281), corresponding to a shift of 0.08 Å from the ideal position of y = 0.25. This type of pseudo-symmetry can best be described by applying an origin shift of $(0\frac{1}{4}\frac{1}{4})$ to the coordinates of the network atoms. Table 6 exhibits the coordinates of Ti(1) as an example; its eightfold position can also be constructed by applying the symmetry operations of the non-standard space group *F2/m* to the special position (*x*0*z*), with site symmetry **m**. These considerations can be extended to all network atoms. Therefore, the space group of the network substructure can be taken as approximately *F2/m* using the standard space group notation, which corresponds to *C2/m* with a transformed unit cell of half the volume. The incorporation of the Bi cations in the channels is responsible for the loss of the face centring and of the mirror plane. The symmetry is reduced to *C2/c*.

Phase transition and structure of β-$Bi_2Ti_4O_{11}$

High-temperature powder diffraction experiments indicate a reversible phase transformation at the transition temperature T_c = 505 K (see Fig. 3). A DSC measurement of the same material is also in good agreement with this value (T_c = 506.48 K). The diffraction lines not affected by the phase transformation were of the type (*ooo*) or (*eee*) (*o* = odd, *e* = even).

This result indicates that the transition is characterized by the development of face centring. Precession photographs taken at a temperature of 573 K showed monoclinic symmetry. In correspondence to the powder investigations, the general absences $h + k = 2n + 1$, $k + l = 2n + 1$, $h + l = 2n + 1$ were confirmed. Leaving the unit-cell dimensions of the α-phase unchanged, the absences result in an extinction symbol $F1 - 1$ for β-$Bi_2Ti_4O_{11}$, which can be transformed to $C1 - 1$ with possible space groups *C*2, *Cm* and *C2/m* using the new axes $\mathbf{a}' = \mathbf{a}$, $\mathbf{b}' = \mathbf{b}$, $\mathbf{c}' = (\mathbf{c} - \mathbf{a})/2$. The volume of this new cell is diminished by a factor of two.

From the close relation between the two cells of the pseudo-symmetric substructure of the network in α-$Bi_2Ti_4O_{11}$ on the one hand, and the β-phase on the other, we infer that the phase transition is of a displacive nature and primarily due to a displacement of the Bi cations, whereas the Ti and O atoms basically remain at their positions. Starting from this assumption the coordinates of the atoms in the α-phase were transformed to special positions of *C2/m*: 4(*i*) or 2(*b*) [for O(3)]. The full-matrix least squares refinement based on this model with 29 variable parameters converged to a final weighted residual of wR = 0.0432, including anisotropic displacement factors for all atoms. Tables 7–10 contain the coordinates, temperature coefficients and the calculated bond lengths and angles. As in the α-phase, the TiO_6-octahedra around Ti(1) show greater variation in the Ti—O distances than the Ti(2)-octahedra, whereas the mean bond lengths of both octahedra are now almost identical (1.955 and 1.956 Å).

The formal coordination of Bi increases from 11 to 12. The distinction between an inner and outer coordination sphere becomes more pronounced with five O atoms within 2.464 Å and the next furthest O atoms 3.141 Å apart.

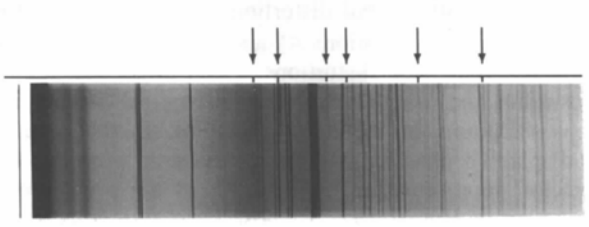

Fig. 3. Part of a Guinier film lift photograph showing the disappearance of the lines (110), ($\bar{1}$12), ($\bar{3}$12), ($\bar{1}$14), (512) and (316).

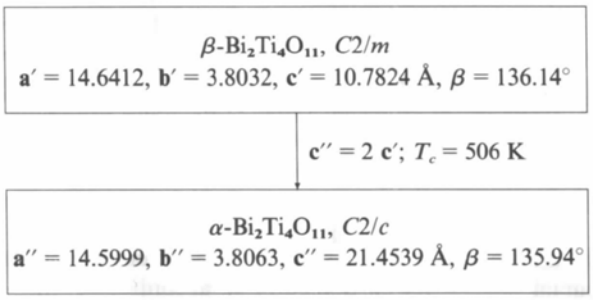

Table 8. *Anisotropic displacement parameters* ($Å^2$) *for* β-$Bi_2Ti_4O_{11}$

	U_{11}	U_{22}	U_{33}	U_{12}	U_{13}	U_{23}
Bi	0.0171 (2)	0.0400 (4)	0.0162 (2)	0	0.0137 (2)	0
Ti(1)	0.0075 (8)	0.0061 (10)	0.0068 (7)	0	0.0054 (7)	0
Ti(2)	0.0082 (7)	0.0056 (10)	0.0068 (7)	0	0.0054 (7)	0
O(1)	0.0183 (38)	0.0100 (38)	0.0150 (35)	0	0.0134 (33)	0
O(2)	0.0198 (41)	0.0097 (49)	0.0165 (38)	0	0.0155 (37)	0
O(3)	0.0197 (58)	0.0320 (93)	0.0088 (46)	0	0.0122 (48)	0
O(4)	0.0043 (29)	0.0240 (56)	0.0034 (28)	0	0.0020 (26)	0
O(5)	0.0061 (36)	0.0319 (64)	0.0107 (35)	0	0.0018 (33)	0
O(6)	0.0083 (31)	0.0114 (46)	0.0102 (32)	0	0.0067 (29)	0

Table 9. *Interatomic distances up to a maximum of* 3.4 Å *for* β-$Bi_2Ti_4O_{11}$

Ti(1)—O(1)	1.951 (1)	Bi—O(1)	3.146 (8)
Ti(1)—O(5)	1.789 (6)	Bi—O(3)	3.368 (1)
Ti(1)—O(1)	1.951 (1)	Bi—O(5)	3.141 (5)
Ti(1)—O(6)	2.195 (7)	Bi—O(2)	3.299 (9)
Ti(1)—O(2)	2.095 (7)	Bi—O(4)	2.464 (4)
Ti(1)—O(3)	1.847 (1)	Bi—O(6)	2.143 (4)
Ti(2)—O(1)	1.996 (8)	Bi—O(2)	3.299 (7)
Ti(2)—O(4)	2.018 (4)	Bi—O(4)	2.464 (4)
Ti(2)—O(2)	1.925 (1)	Bi—O(6)	2.410 (5)
Ti(2)—O(5)	1.884 (7)	Bi—O(3)	3.368 (1)
Ti(2)—O(2)	1.925 (1)	Bi—O(5)	3.141 (5)
Ti(2)—O(4)	1.989 (6)	Bi—O(6)	2.410 (5)

Table 10. O—Ti—O *angles* (°) *for* β-$Bi_2Ti_4O_{11}$

O(1)—Ti(1)—O(1)	154.2 (2)	O(1)—Ti(2)—O(2)	81.4 (2)
O(1)—Ti(1)—O(3)	100.3 (2)	O(1)—Ti(2)—O(4)	171.3 (2)
O(1)—Ti(1)—O(5)	96.7 (2)	O(2)—Ti(2)—O(4)	88.6 (2)
O(2)—Ti(1)—O(3)	167.8 (2)	O(2)—Ti(2)—O(4)	98.3(2)
O(3)—Ti(1)—O(5)	95.1 (3)	O(4)—Ti(2)—O(4)	78.3 (3)
O(1)—Ti(1)—O(2)	78.3 (2)	O(1)—Ti(2)—O(2)	81.4 (2)
O(1)—Ti(1)—O(3)	100.3 (2)	O(1)—Ti(2)—O(5)	104.1 (3)
O(1)—Ti(1)—O(6)	83.3 (2)	O(2)—Ti(2)—O(4)	88.6 (2)
O(2)—Ti(1)—O(6)	82.8 (3)	O(2)—Ti(2)—O(5)	93.9 (2)
O(3)—Ti(1)—O(6)	85.0 (2)	O(4)—Ti(2)—O(5)	84.6 (3)
O(1)—Ti(1)—O(2)	78.3 (2)	O(1)—Ti(2)—O(4)	93.0 (3)
O(1)—Ti(1)—O(5)	96.7 (2)	O(2)—Ti(2)—O(2)	162.3 (3)
O(1)—Ti(1)—O(6)	83.3 (2)	O(2)—Ti(2)—O(4)	98.3 (2)
O(2)—Ti(1)—O(5)	97.1 (3)	O(2)—Ti(2)—O(5)	93.9 (2)
O(5)—Ti(1)—O(6)	180.0 (3)	O(4)—Ti(2)—O(5)	162.9 (3)

Symmetry analysis and microscopic distortions

In order to investigate the symmetry relations between the two phases of $Bi_2Ti_4O_{11}$, the unit cell of the α-phase employed in the structure determination is transformed to a cell of equal volume according to $\mathbf{a}'' = \mathbf{a}$, $\mathbf{b}'' = \mathbf{b}$, $\mathbf{c}'' = -\mathbf{a} + \mathbf{c}$. The transition can then be described as a result of doubling the $\mathbf{c}'$ lattice constant.

The characteristic wave vector of the transition $A = (00\frac{1}{2})$ lies on the boundary of the first Brillouin zone. The symmetry reduction from the high- to the low-temperature phase is initiated by a loss in translational symmetry and no loss of point symmetry. According to Toledano & Toledano (1987), the transition can be classified as non-ferroic. Further information on the transition can be drawn from the tables of Stokes & Hatch (1988). A phase transition from $C2/m$ to $C2/c$ coupled with a doubling of the c lattice constant can be induced from the onset of a one-dimensional order parameter $\eta = (0\delta0)$, transforming according to one of the irreducible representations A_1^- or A_2^+. Both representations fulfil the Landau and Lifshitz criteria for a continous transformation. For A_2^+, the subgroup $C2/c$ is obtained directly from $C2/m$ without any origin shift. The $C2/c$ structure inferred from A_1^- requires a shift of $(0\frac{1}{2}0)$ in order to obtain the standard notation given in the *International Tables for Crystallography* (1983). Although the two order parameters connected with A_2^+ and A_1^- result in the same space-group symmetry $C2/c$, they differ in their transformation behaviour with respect to the symmetry elements of the higher symmetric space group $C2/m$ of the β-phase. The two possible phases with $C2/c$ symmetry represent different structures because the microscopic distortions associated with the order parameters are different.

Up to this point we have considered the transformation only in terms of the symmetry properties of $C2/m$ to $C2/c$; we did not attempt to specify the distortions that cause the loss in symmetry. In the course of the following discussion we will show that the irreducible representation A_2^+ is responsible for the phase transition and describe the distortions that bring about the space group change, choosing the displacements of the Bi cations in the [010] direction as a primary order parameter. The Bi atoms are located at the 4(i) Wyckoff positions with site symmetry **m**. Each of the (i) sites, $(x0y)$, $(\bar{x}0\bar{z})$, plus their C-centred translations, will be left unchanged by the respective site symmetry group, a subgroup of $C2/m$ that is isomorphic to the point group **m**. For example, the Bi in $(x0y)$ is invariant under a group consisting of the elements $[(x,y,z), (x,\bar{y},z,)]$. Using the results of Hatch, Stokes & Putnam (1987), an induced representation of $C2/m$ can be obtained from the irreducible representations of this group. Distortions for all equivalent sites can be inferred from projection operator methods (Stokes, Hatch & Wells, 1991). In this manner, the global distortions characterized by the irreducible representations A_2^+ and A_1^- of $C2/m$ are constructed from local distortions which effect the atomic positions and which are classified by the irreducible representations of the point group **m**. In the case of a displacive phase transition, we have to consider the 'vector' representations $\mathbf{A}'$ and $\mathbf{A}''$ of the point group [notation of Burns (1977)] whose basis functions transform like components of vectors representing atomic displacements. This process is similar to the way in

Table 11. *Displacements along* [010] *for Wyckoff position* 4(*i*)

IR	Position	No.	Displacement	Position	No.	Displacement
A_2^+	$(x, 0, z)$	1	$(0, -\delta, 0)$	$(x, 0, z+1)$	5	$(0, +\delta, 0)$
	$(\bar{x}, 0, \bar{z})$	2	$(0, +\delta, 0)$	$(\bar{x}, 0, \bar{z}+1)$	6	$(0, -\delta, 0)$
	$(x+\frac{1}{2}, \frac{1}{2}, z)$	3	$(0, -\delta, 0)$	$(x+\frac{1}{2}, \frac{1}{2}, z+1)$	7	$(0, +\delta, 0)$
	$(\bar{x}+\frac{1}{2}, \frac{1}{2}, \bar{z})$	4	$(0, +\delta, 0)$	$(\bar{x}+\frac{1}{2}, \frac{1}{2}, \bar{z}+1)$	8	$(0, -\delta, 0)$
A_1^-	$(x, 0, z)$	1	$(0, +\delta, 0)$	$(x, 0, z+1)$	5	$(0, -\delta, 0)$
	$(\bar{x}, 0, \bar{z})$	2	$(0, +\delta, 0)$	$(\bar{x}, 0, \bar{z}+1)$	6	$(0, -\delta, 0)$
	$(x+\frac{1}{2}, \frac{1}{2}, z)$	3	$(0, +\delta, 0)$	$(x+\frac{1}{2}, \frac{1}{2}, z+1)$	7	$(0, -\delta, 0)$
	$(\bar{x}+\frac{1}{2}, \frac{1}{2}, \bar{z})$	4	$(0, +\delta, 0)$	$(\bar{x}+\frac{1}{2}, \frac{1}{2}, \bar{z}+1)$	8	$(0, -\delta, 0)$

Table 12. *Displacements of the Bi atoms along* [010]

	Coordinates in *C2/m*				Coordinates in *C2/c*			
No.	*x*	*y*	*z*	Cell	*x*	*y*	z	Displacements
1	0.2509	0	0.1421	I	0.1788	0.1748	0.8203	$\frac{1}{4} - \delta$
2	0.7491	0	0.8579	I	0.3212	0.3252	0.1797	$\frac{1}{4} + \delta$
3	0.7509	$\frac{1}{2}$	0.1421	I	0.6788	0.6748	0.8203	$\frac{3}{4} - \delta$
4	0.2491	$\frac{1}{2}$	0.8579	I	0.8212	0.8252	0.1797	$\frac{3}{4} + \delta$
5	0.2509	0	1.1421	II	0.6788	0.3252	0.3203	$\frac{1}{4} + \delta$
6	0.7491	0	1.8579	II	0.8212	0.1748	0.6797	$\frac{1}{4} - \delta$
7	0.7509	$\frac{1}{2}$	1.1421	II	0.1788	0.8252	0.3203	$\frac{3}{4} + \delta$
8	0.2491	$\frac{1}{2}$	1.8579	II	0.3212	0.6784	0.6797	$\frac{3}{4} - \delta$

which lattice modes are calculated. The results of our calculations for A_2^+ and A_1^- are summarized in Table 11. Two atoms having the same sign in the component δ of the relative displacement vector along [010] are displaced in the same direction.

An opposite sign in δ indicates an antiparallel displacement. In order to relate the Bi-displacements in α-$Bi_2Ti_4O_{11}$ from positions of the β-phase to one of the irreducible representations, corresponding atoms are shown in Table 12 for comparison.

The coordinates of the atoms in the α-phase are given in terms of the pseudo-tetragonal unit cell used in the structure refinement. The Bi cation No. 1, for example, with coordinates (0.2509,0,0.1421) will be transformed to the position $(0.1788, \frac{1}{4}, 0.8203)$, in addition, the phase transition leads to a displacement of $\delta = 0.075$ (*ca* 0.29 Å) along $[0\bar{1}0]$. Compared with the results of Table 11, it is obvious that the distortion pattern in α-$Bi_2Ti_4O_{11}$ is explained by means of a transition according to the A_2^+ representation. Two subcells, I and II, containing the atoms 1–4 and 5–8, respectively, can be distinguished. Corresponding atoms show an antiparallel displacement and thus an antiferroelectric polarization state results in α-$Bi_2Ti_4O_{11}$ (see Fig. 4).

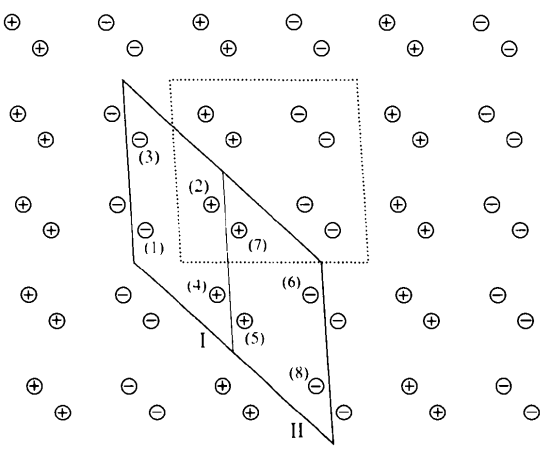

Fig. 4. Bi-substructure in a projection along [010]. The stippled pseudo-tetragonal cell was used in the structure refinement ; the bold-faced cell corresponds to the cell employed for the description of the phase transition.

The project has been supported by a grant of the Deutsche Forschungsgemeinschaft; local support was given by the Materialwissenschaftliches Forschungszentrum der Universität Mainz.

References

ANDERSSON, S. & WADSLEY, A. D. (1962). *Acta Cryst.* **15**, 194–201.

BARSUKOVA, M. L., KUZNETSOV, V. A., LOBACHEV, A. N. & TANAKINA, T. N. (1973). *Sov. Phys. Crystallogr.* **17**, 739–742.

BAUR, W. H., WENNINGER, G., ROY, S. D. & KASSNER, D. (1986). *SADIAN*91. Univ. Frankfurt, Germany.

BURNS, G. (1977). *Introduction to Group Theory with Applications*. New York: Academic Press.

Enraf–Nonius. (1990). *MolEN. An Interactive Intelligent System for Crystal Structure Analysis*. Enraf–Nonius, Delft, The Netherlands.

FISCHER, R. X., LELIRZIN, A., KASSNER, D. & RÜDINGER, B. (1991). *STRUPLO*90. *Z. Kristallogr.* Suppl. 3, 75.

HATCH, D. M., STOKES, H. T. & PUTNAM, R. M. (1987). *Phys. Rev. B*, **35**, 4935–4942.

HISANO, K. & TODA, K. (1977). *Solid State Commun.* **24**, 247–251.

IBERS, J. A. & HAMILTON, W. C. (1974). *International Tables for X-ray Crystallography*, Vols. I–IV. Birmingham: Kynoch Press.

KAHLENBERG, V. & BÖHM, H. (1992). *Hasylab Jahresbericht*, pp. 617–618.

MITROVICH, L. V. & BLINOV, V. A. (1982). *Fiz.-Khim. Issled. Strukt. Svoistv. Stekol Steklokrist. Mater.* pp. 18–22.

PAMPLIN, B. R. (1974). *Crystal Growth*. Oxford: Pergamon Press.

PETUSHKOVA, L. V., DMITRIEVA, S. P., POBEDIMSKAYA, E. V. & BELOV, N. V. (1974). *Sov. Phys. Dokl.* **19**, 263–265.

SHELDRICK, G. M. (1976). *SHELX76. Program for Crystal Structure Determination.* Univ. of Cambridge, England.
SHIMADA, S., KODAIRA, K. & MATSUSHITA, T. (1977). *J. Cryst. Growth*, **41**, 317–320.
STOKES, H. T. & HATCH, D. M. (1988). *Isotropy Subgroups of the 230 Space Groups*. Singapore: World Scientific.
STOKES, H. T., HATCH, D. M. & WELLS, J. D. (1991). *Phys. Rev. B*, **43**, 11010–11018.
SUBBARAO, E. C. (1962). *J. Am. Ceram. Soc.* **45**, 564–565.
TILLMANNS, E. (1974). *Acta Cryst.* B**30**, 2894–2896.
TILLMANNS, E., HOFMEISTER, W. & BAUR, W. H. (1985). *J. Solid State Chem.* **58**, 14–28.
TOLEDANO, J. C. & TOLEDANO, P. (1987). *The Landau Theory of Phase Transitions*. Singapore: World Scientific.
TUINSTRA, F. & STORM, G. M. (1978). *J. Appl. Cryst.* **11**, 257–259.
WELLS, A. F. (1984). *Inorganic Chemistry*. Oxford: Clarendon Press.

Acta Cryst. (1995). B**51**, 18–22

Single Crystal Study of the 'BaSr' 1212 Superconductor $Tl_{1+x}BaSrCa_{1-x}Cu_2O_{7-\delta}$

BY PH. LABBÉ, M. LEDÉSERT, A. MAIGNAN, C. MARTIN, H. LELIGNY AND B. RAVEAU

Laboratoire CRISMAT, ISMRA-Université de Caen, Boulevard du Maréchal Juin 14050, *Caen CEDEX, France*

(*Received* 7 *February* 1994; *accepted* 4 *May* 1994)

Abstract

Single crystals of the 'BaSr' thallium cuprate $Tl_{1+x}BaSrCa_{1-x}Cu_2O_{7-\delta}$ have been grown for the first time. The structure parameters of this tetragonal phase were successively refined using four single-crystal X-ray diffraction data of the same crystal, as-grown [$T_c = 62$ K, $a = 3.8271$ (7), $c = 12.385$ (3) Å] and after different thermal treatments: two annealings under H_2/Ar flow [$T_c = 90$ K, $a = 3.8356$ (7), $c = 12.390$ (3) Å] and one under oxygen pressure $P_{O_2} = 100$ bar [$T_c = 60$ K, $a = 3.8234$ (9), $c = 12.384$ (4) Å]. The corresponding results provided evidence of a reversible evolution of the cation oxygen distances and of the thallium splitting depending on the reducing/oxidizing conditions of annealing which are well correlated to the superconducting properties. A relationship between T_c's of this $Tl_{1.22}Ba_{1.04}Sr_{0.96}Ca_{0.78}Cu_2O_{7-\delta}$ 'BaSr' 1212 crystal and Cu—Cu distances is compared with the results obtained for pure 'Ba' and 'Sr' 1212 phases.

Introduction

Numerous investigations have been performed on the layered thallium cuprates owing to their critical temperature (T_c) which covers a wide range up to 130 K. Their high sensitivity to the nature of the annealing atmosphere at low temperature (Hervieu *et al.*, 1988; Shimakawa *et al.*, 1989; Martin *et al.*, 1990; Morosin, Baughman, Ginley, Schirber & Venturini, 1990) has shown that the hole carrier density is a predominant factor in the optimization of the critical temperature of these materials. Although the influence of oxygen non-stoichiometry upon T_c's is well established, the relationships between the structure, chemical bonding and superconductivity is so far not understood. This is, for instance, the case with the thallium 1212-cuprates $Tl_{1+x}Ba_2Ca_{1-x}Cu_2O_{7-\delta}$ (Morosin *et al.*, 1988; Morosin, Baughman, Ginley, Schirber & Venturini, 1990) and $Tl_{1+x}Sr_2Ca_{1-x}Cu_2O_{7-\delta}$ (Izumi *et al.*, 1991) that exhibit very different T_c's of 103 (Morosin *et al.*, 1988) and 58 K (Izumi *et al.*, 1991), respectively, in spite of their very similar chemical composition, $x = 0.17$–0.12 and $\delta = 0.25$–0.22. This would imply mean oxidation states of copper of 2.16 and 2.24 for the Ba and Sr phases, respectively, suggesting that the latter is overdoped with respect to the barium cuprate. Nevertheless, all attempts to increase the T_c's of the Sr phase by annealing in reducing conditions did not allow a T_c higher than 68 K to be obtained (Kubo, Kondo, Shimakawa, Manako & Igarashi, 1992). In order to understand this behaviour, mixed 'BaSr' 1212 cuprates were recently synthesized with critical temperatures ranging from 20 to 100 K (Maignan *et al.*, 1993). There is no doubt that to get the clue to such an issue, accurate crystal data about structure, composition and superconducting properties have to be accumulated. We report here on the structure of a unique single crystal of the mixed-phase $Tl_{1+x}BaSrCa_{1-x}Cu_2O_{7-\delta}$, submitted to different thermal treatments in H_2–Ar flow and under oxygen pressure. This investigation is completed by a magnetic study of a crystal of similar parameters, with the same cationic composition.

Experimental

The preparation of '1212' crystals was similar to that previously reported (Martin *et al.*, 1993) for the '1223' $Tl(Ba,Sr)_2Ca_2Cu_3O_9$ crystals. Appropriate